Stable Vacua with Realistic Phenomenology and Cosmology in Heterotic M-theory Satisfying Swampland Conjectures

Cedric Deffayet, Burt A Ovrut, Paul J Steinhardt

Published for SISSA by Springer

Received: March 2, 2024
Revised: May 21, 2024
Accepted: July 6, 2024
Published: July 31, 2024

Stable vacua with realistic phenomenology and cosmology in heterotic M-theory satisfying Swampland conjectures

Cédric Deffayet,[a] **Burt A. Ovrut**[b] **and Paul J. Steinhardt**[c,d]

[a] *Laboratoire de Physique de l'Ecole Normale Supérieure, ENS, Université PSL, CNRS, Sorbonne Université, Université Paris Cité, F-75005 Paris, France*

[b] *Department of Physics, University of Pennsylvania, Philadelphia, PA 19104, U.S.A.*

[c] *Department of Physics, Princeton University, Princeton, New Jersey 08544, U.S.A.*

[d] *Jefferson Physical Laboratory, Harvard University, Cambridge MA 02138 U.S.A.*

E-mail: cedric.deffayet@phys.ens.fr, ovrut@elcapitan.hep.upenn.edu, steinh@princeton.edu

Abstract: We recently described a protocol for computing the potential energy in heterotic M-theory for the dilaton, complex structure and Kähler moduli. This included the leading order non-perturbative contributions to the complex structure, gaugino condensation and worldsheet instantons assuming a hidden sector that contains an anomalous U(1) structure group embedded in E_8. In this paper, we elucidate, in detail, the mathematical and computational methods required to utilize this protocol. These methods are then applied to a realistic heterotic M-theory model, the $B-L$ MSSM, whose observable sector is consistent with all particle physics requirements. Within this context, it is shown that the dilaton and universal moduli can be completely stabilized at values compatible with every phenomenological and mathematical constraint — as well as with ΛCDM cosmology. We also show that the heterotic M-theory vacua are consistent with all well-supported Swampland conjectures based on considerations of string theory and quantum gravity, and we discuss the implications of dark energy theorems for compactified theories.

Keywords: Axions and ALPs, String and Brane Phenomenology, Superstrings and Heterotic Strings

ArXiv ePrint: 2401.04828

https://doi.org/10.1007/JHEP07(2024)288

JHEP07(2024)288

Contents

1 Introduction

In a recent paper [1], we discussed stabilizing the dilaton, complex structure and Kähler moduli in heterotic M-theory vacua that are consistent with presently well-supported Swampland conjectures in the limit of large moduli fields. A major challenge for string theory is that it predicts a vast landscape of potential vacua, most of which are incompatible with particle physics experiments and cosmological observations. Brute force analysis of the full landscape to identify which vacua are consistent with observations does not appear to be practical. Furthermore, simpler approaches based on supergravity and effective field theory may also be unproductive, since they admit an abundance of models that are incompatible with string theory and quantum gravity, as suggested by Swampland studies [2–6]. A more modest but potentially more productive approach has been to try to construct explicit models directly from heterotic M-theory, following the highly non-trivial, elaborate methodology for compactifying eleven to (3+1)-dimensions [7–10]. There is a large literature in this context — mainly constructing the MSSM and other phenomenologically acceptable vacua on the observable sector — see, for example [11–17]. However, an important requirement of any such vacuum is to demonstrate the stability of the dilaton, complex structure and Kähler moduli. This has been studied for a wide variety of superstring vacua in [18–23]. A careful and precise protocol for doing this within the context of heterotic M-theory was recently presented in [1]. However, several of the mathematical and analytic procedures used require further in-depth

JHEP07(2024)288

presentation. Furthermore, it is important to show that it is possible to find at least one such vacuum that has both phenomenologically and cosmologically acceptable low energy physics.

This paper is an attempt to satisfy both requirements. First, the mathematical and analytic subtleties used in [1] will be elucidated in detail. Secondly, using the protocol presented in [1], a *modest* attempt to present an explicit model that satisfies all phenomenological and cosmological constraints will be presented. This is a modest attempt because, even within the formalism presented in [1], it is not currently known how to compute certain details of compactification. For now, our only option is to parameterize these uncertainties based on mathematically plausible constraints. As shown in [1], the results are instructive and promising. In this paper, we demonstrate with an explicit example that it is possible (subject to the uncertainties noted above) to construct models based on heterotic M-theory that contain a stable vacuum with fixed moduli, a visible sector with realistic standard model physics, and a vacuum energy consistent with ΛCDM cosmology.

The paper is organized as follows: section 2 reviews the general procedure described in [1] for deriving the D-term and F-term contributions to the potential energy (V_D and V_F, respectively), for the dilaton, complex structure moduli, and Kähler moduli in heterotic M-theory. As argued in [1], the minima of the total potential satisfy $V_D = 0$. What remains is to minimize V_F subject to this constraint. Section 3 describes the numerical procedure used to search for minima of V_F in which all the moduli are stabilized and to determine the range of possible potential shapes as parameters are varied. Section 4 then demonstrates that this construction can be enhanced with a visible sector that results in realistic particle phenomenology and ΛCDM cosmology. For this example, we choose the heterotic M-theory $B-L$ MSSM model. Section 5 discusses some of the implications of this work for Swampland conjectures and quantum gravity [2–6]; for related dark energy theorems for compactified theories [24–26]; and for axion-based cosmology. We want to emphasize that the moduli stabilized $B-L$ MSSM vacua presented here are consistent with all presently well-supported Swampland conjectures.

Finally, we want to point out that all results in this paper are calculated to leading order in both the perturbative and non-perturbative superpotentials arising in the theory. That is, although supersymmetry is spontaneously broken by gaugino condensation at the stabilized moduli vacua presented, higher order perturbative corrections due to this supersymmetry breaking–which are expected to be relatively suppressed–will be ignored.

2 Deriving the potential energy

A step-by-step procedure for deriving the potential energy V for the dilaton, complex structure moduli and Kähler moduli in heterotic M-theory vacua where the hidden sector contains an anomalous U(1) gauge group was presented in detail in [1]. For simplicity, the dimensions of the relevant cohomologies of the compactification Calabi-Yau threefold X were chosen to be $h^{1,1} = h^{2,1} = 1$. However, the results apply to the "universal" geometric moduli of theories with $h^{1,1}, h^{2,1} > 1$ as well.

In this section, we present a brief review of that procedure. First, one constructs the F-term potential energy, V_F. To do this, begin by considering the complex structure moduli of z^a, $a = 1, \ldots, h^{2,1}$. For arbitrary $h^{2,1} \geq 1$, the Kähler potential, $\mathcal{K}$ and superpotential,

JHEP07(2024)288

W_{flux} are well known [27, 28]. However, here, as in [1], we limit the analysis to Calabi-Yau threefolds with $h^{2,1} = 1$. The resulting potential energy, V_{flux}, has a countably infinite set of local minima with unbroken $N = 1$ supersymmetry. We, henceforth, will assume that the complex structure modulus z is fixed to be in one of these supersymmetry preserving vacua.

The second step is to include the complex dilaton field S with the associated Kähler potential K_S. One then assumes that the commutant in E_8 of the anomalous U(1) structure group contains a non-Abelian group that becomes strongly coupled near the compactification mass scale M_U. This induces a non-perturbative superpotential W_G through gaugino condensation [29–32].

The third step, since $h^{1,1} = 1$, is to introduce the universal Kähler modulus T with the known Kähler potential K_T, as well as the associated non-perturbative "worldsheet" instanton superpotential W_T [33–38]. The superpotential results from wrapping a string around each isolated, genus-zero, holomorphic curve C_i, the number of which is given by the Gromov-Witten invariant. Summing over all such curves leads to the instanton superpotential of exponential form $W_T = M_U^3 \, (pe^{i\theta_p}) \, e^{-\tau T}$, where $pe^{i\theta_p}$ is the complex-valued "Pfaffian" factor (with magnitude p and phase θ_p). The Pfaffian is a holomorphic function of vector bundle moduli evaluated at each isolated curve C_i and then summed over all such curves [39, 40]. This sum has been shown to be non-vanishing for a large number of heterotic string vacua [41–46] — which we assume henceforth. The full F-term potential energy V_F was then computed from the combined superpotential $W = W_{flux} + W_G + W_T$ using the associated Kähler potentials.

Next, a separate D-term potential V_D, which is generated by the inhomogeneous transformations of the S and T moduli "axions"under the anomalous U(1) structure group [47, 48], must be added. These inhomogeneous transformations arise from the Green-Schwarz mechanism [49] required to cancel the U(1) anomaly. V_D, whose exact form can be found in [50], is a non-negative function of $s = Re\, S$ and $t = Re\, T$. V_D is minimal, in fact precisely zero, along a specific direction in field space, $s = const. \times t$, where the proportionality constant is a fixed function of various parameters of the chosen vacuum. Since the scalar fields along this specific direction minimize V_D, we will henceforth write them as $\langle s \rangle$ and $\langle t \rangle$ despite the fact that $\langle s \rangle \propto \langle t \rangle$ have not yet been determined. By constraining s and t to lie along the "D-flat direction" (referred to as setting the Fayet-Iliopouos term to zero or $FI = 0$), V_D does not break $N = 1$ supersymmetry. Hence, in the full potential energy $V = V_D + V_F$, supersymmetry breaking is due entirely to gaugino condensation at the compactification scale M_U [51].

Since the D-flat direction corresponds to an absolute minimum of V_D, the search for the minima of the combined potential $V = V_F + V_D$ can be confined to values of S and T along $\langle s \rangle = const. \times \langle t \rangle$. Furthermore, the complex perturbations of S and T around any point along the D-flat direction can be unitarily rotated to two new complex fields, ξ^1 and ξ^2, that have canonical kinetic energy and are mass eigenstates. The mass of ξ^1 is non-zero and given by the anomalous mass m_{anom} of the U(1) vector boson. For choices of parameters and $\langle t \rangle$ for which $m_{anom} \geq M_U$, the U(1) vector superfield and chiral superfield ξ^1 can be "integrated out" of the low energy effective Lagrangian. However, the second diagonalized complex scalar ξ^2, with real and imaginary components η and ϕ respectively, has canonical kinetic energy and much smaller masses, m_η and m_ϕ, so they must be included in the low energy potential V.

After these steps, and using the fact that $V_D = 0$ along the D-flat direction, minimizing the total potential energy amounts to minimizing V_F subject to the constraint $\langle s \rangle = const. \times \langle t \rangle$.

JHEP07(2024)288

More specifically, it was shown in [1] that the D-flat direction of V_D is given by

$$\langle s\rangle = 0.230 F^{4/3}\beta\langle t\rangle\,, \tag{2.1}$$

where the coefficient F parameterizes the ratio of the length scale $\pi\rho$ of the fifth dimension of the vacuum to five times $v^{1/6}$, where v sets the scale of the volume of the Calabi-Yau threefold, and β is the gauge charge on the observable sector. V_F is then reduced to a function of $\langle t\rangle$ and the fields ϕ and η:

$$\begin{aligned}
V_F(\langle t\rangle,\tilde{\eta},\tilde{\phi}) = {} & \frac{M_U^4}{F^{4/3}\beta\langle t\rangle^4\,\langle c\rangle^3\,(0.230{+}1.15\tilde{\phi})(1{+}5.00\tilde{\phi})^3} \\
& \times\Bigg\{1.14\,\frac{(A^2{+}B^2)}{F^{4/3}} \\
& +1.32\times10^{-6}\big((1{+}19.0F^{2/3}\beta\langle t\rangle(1{+}5.01\tilde{\phi})^2{+}3\big) \\
& \quad\times\exp[-19.0\,F^{2/3}\beta\langle t\rangle(1{+}5.01\,\tilde{\phi})] \\
& -(2.43\times10^{-3}F^{-2/3})\,(1{+}19.0\,F^{2/3}\beta\langle t\rangle(1{+}5.01\,\tilde{\phi})) \\
& \quad\times\exp[-9.48\,F^{2/3}\beta\langle t\rangle(1{+}5.00\,\tilde{\phi})] \\
& \quad\times sgn(A)\sqrt{A^2{+}B^2}\cos[47.5\,F^{2/3}\beta\langle t\rangle\tilde{\eta}-\ \arctan(\frac{B}{A})] \\
& +2.62\times10^{-6}\,p\,(5.5{+}\langle t\rangle(19.0\,F^{2/3}\beta(1{+}5.01\,\tilde{\phi}){+}3\tau(1{+}5.00\,\tilde{\phi}))) \\
& \quad\times\exp[-(9.49\,F^{2/3}\beta(1{+}5.011\,\tilde{\phi}){+}\tau(1{+}5.00\,\tilde{\phi}))\langle t\rangle] \\
& \quad\times\cos[(-47.5\,F^{2/3}\beta{+}5.00\,\tau)\langle t\rangle\tilde{\eta}{+}\theta_p] \\
& +4.36\times10^{-7}p^2\big(3{+}(3{+}2\,\tau\langle t\rangle(1{+}5.00\,\tilde{\phi}))^2\big) \\
& \quad\times\exp[-2\tau\langle t\rangle(1{+}5.00\,\tilde{\phi})] \\
& -2.43\times10^{-3}\,F^{-2/3}\,p\,(1{+}2\tau\langle t\rangle(1{+}5.00\,\tilde{\phi})) \\
& \quad\times\exp[-\tau\langle t\rangle(1{+}5.00\,\tilde{\phi})] \\
& \quad\times sgn(A)\sqrt{A^2{+}B^2}\cos[5.00\,\tau\langle t\rangle\tilde{\eta}{+}\theta_p-\ \arctan(\frac{B}{A})]\Bigg\}
\end{aligned} \tag{2.2}$$

where $\tilde{\eta} = \eta/M_P$ and $\tilde{\phi} = \phi/M_P$, $M_P = 1.22\times10^{19}\,\text{GeV}$ is the four dimensional Planck mass, and the unification scale is canonically fixed to $M_U = 3.15\times10^{16}\,\text{GeV}$ [52, 53]. The coefficients A, B and $\langle c\rangle$ are set by the choice of the $N=1$ supersymmetric minimum of V_{flux}.

It was shown in [1] that

$$m_{\text{anom}} = 3.38\,l\,M_U/(F\beta^{1/2}\langle t\rangle^{3/2})\,, \tag{2.3}$$

where l is an integer that defines the line bundle. As discussed above, our expression for V_F given in (2.2) is valid provided $m_{\text{anom}} \geq M_U$; or, equivalently, V_F given in (2.2) is only valid for

$$\langle t\rangle < \langle t\rangle_{bound} \equiv \left(\frac{3.38\,l}{F\beta^{1/2}}\right)^{2/3}\,. \tag{2.4}$$

JHEP07(2024)288

3 Potential energy minima

Before adding a visible sector to the heterotic M-theory construction above, we search for a parameter range consistent with our physical approximations for which there exist stable or long-lived metastable vacuum states. We have argued that the minima lie along the D-flat direction, along which $\langle s \rangle$ is proportional to $\langle t \rangle$ and V_D is at its absolute minimum and equal to zero. What remains is to find the minima of $V_F(\langle t \rangle, \tilde{\eta}, \tilde{\phi})$ in eq. (2.2) satisfying eq. (2.4) as a function of the parameters. In principle, one could invoke a brute force numerical code for this purpose. However, it is more instructive to take steps to simplify the problem before turning to numerics. We then check our results by substituting our answers into the original expression and confirming our conclusions.

The following approach proves to be effective:

1. *Reduce the degrees of freedom by setting $\tilde{\phi} = 0$:* by construction, $\tilde{\phi}$ is a perturbation away from any minimum we find along the $\langle s \rangle = const.\langle t \rangle$ D-flat direction, so it's expectation value at the minimum must be zero. Furthermore, as a check for consistency, we compute the squared mass $m_{\tilde{\phi}}^2$ of the perturbation $\tilde{\phi}$ about any minimum we may find, and show that it is always positive.

2. *Simplify V_F by ignoring numerically negligibly terms:* of the six terms within the braces in eq. (2.2), the numerical values of the second, third and fourth terms are negligible compared to the rest because they include a suppression factor of the form $e^{-\alpha\langle t \rangle}$, where α is a large positive coefficient. The first term has no such exponential factor and the fifth and sixth have exponential factors in which α is much smaller. Quantitively, for parameters in the range of interest, the suppression of the second, third and fourth terms compared to the other three terms is by a factor of 10^6 or more, so they can be safely neglected for the purposes of identifying minima.

3. *Reduce the degrees of freedom further by fixing $\tilde{\eta}$:* among the remaining terms — the first, fifth, and sixth in eq. (2.2) — the axion-like field $\tilde{\eta}$ appears only in the sixth term in the argument of the cosine factor. If $A > 0$, $\tilde{\eta}$ has stable minima whenever this argument is such that the cosine is unity; or, equivalently,

$$\langle \tilde{\eta} \rangle = \frac{2\pi n + \arctan(B/A) - \theta_p}{5.00\tau\langle t \rangle} \tag{3.1}$$

   where $n \in \mathbb{Z}$ is any integer. (If $A < 0$, the minimum of $\tilde{\eta}$ shifts by π.) Without loss of generality, we will set $A > 0$ and $n = 0$ in our examples. It follows from eq. (3.1) that the phase θ_p of the Pfaffian factor only shifts $\langle \tilde{\eta} \rangle$, and does not effect V_F at the minimum since the value of the cosine remains unity. Also, a shift in $\langle \tilde{\eta} \rangle$ does not affect the masses of ϕ or η in this approximation.

4. *For a given $\langle t \rangle$, determine if there is a Pfaffian factor p for which $\langle t \rangle$ is an extremum:* an extremum exists if $(\partial V_F/\partial\langle t \rangle)|_{\tilde{\eta}} = 0$, where the subscript signifies that $\tilde{\eta}$ is to be fixed by eq. (3.1) after taking the derivative. Setting $\tilde{\phi} = 0$ and $A > 0$, dropping the second, third and fourth terms and fixing $\langle \tilde{\eta} \rangle$ according to eq. (3.1), the potential

JHEP07(2024)288

reduces to

$$V_F(\langle t\rangle) = \frac{M_U^4}{0.230F^{4/3}\beta\langle t\rangle^4\,\langle c\rangle^3}\Big\{1.14\,F^{-4/3}(A^2+B^2) \\ -2.43\times10^{-3}\,p\,F^{-2/3}\,\sqrt{A^2+B^2}\,(1+2\tau\langle t\rangle)\times\exp[-\tau\langle t\rangle] \\ +4.36\times10^{-7}p^2(3+(3+2\,\tau\langle t\rangle)^2)\times\exp[-2\tau\langle t\rangle]\Big\} \tag{3.2}$$

One can see that V_F is quadratic in p, and the same is true for its derivative:

$$\frac{\partial V_F}{\partial\langle t\rangle}|_{\tilde\eta} = \frac{M_U^4}{F^{8/3}\beta\langle t\rangle^5\,\langle c\rangle^3}\Big\{-19.8(A^2+B^2) \\ +p\,F^{2/3}\sqrt{A^2+B^2}\exp[-\tau\langle t\rangle](0.042+0.07\tau\langle t\rangle+0.021\tau^2\langle t\rangle^2) \\ -\,p^2\,F^{4/3}\exp[-2\tau\langle t\rangle]10^{-4}(0.91+1.1\tau\langle t\rangle+0.61\tau^2\langle t\rangle^2+0.15\tau^3\langle t\rangle^3)\Big\}. \tag{3.3}$$

Therefore, finding a value of p for which $(\partial V_F/\partial\langle t\rangle)|_{\tilde\eta}=0$ entails solving a quadratic equation for p, whose two roots depend on $\langle t\rangle$:

$$p^{1,2}(\langle t\rangle) = \frac{10300\sqrt{A^2+B^2}e^{\tau\langle t\rangle}}{F^{2/3}(6+7.5\tau\langle t\rangle+4\tau^2\langle t\rangle^2+\tau^3\langle t\rangle^3)}\Big[0.042+0.07\tau\langle t\rangle+0.02\tau^2\langle t\rangle^2 \\ \mp10\sqrt{-0.54-0.27\tau\langle t\rangle+0.25\tau^2\langle t\rangle^2+0.19\tau^3\langle t\rangle^3+0.045\tau^4\langle t\rangle^4}\Big], \tag{3.4}$$

where the superscript 1 or 2 corresponds to minus or plus, respectively, in front of the last term within the square brackets.

There is the restriction that the magnitude of the Pfaffian factor, p, must be real and non-negative; or equivalently, the discriminant of the quadratic equation must be non-negative. The discriminant has real coefficients and depends only on τ and $\langle t\rangle$, both of which are real. V_F can only have extrema at $\langle t\rangle$ if there are real combinations of p, τ and $\langle t\rangle$ that satisfy one of the two root equations.

Because β and $\langle c\rangle$ only appear as pre-factors in the expression for the first derivative, the existence or non-existence of extrema and the value of $\langle t\rangle$ at extrema (when they do exist) does not depend on either parameter. Furthermore, after substituting the expressions for $p^{1,2}(\langle t\rangle)\propto\sqrt{A^2+B^2}/F^{2/3}$ into eq. (3.3), the first derivative of V_F factorizes,

$$\frac{\partial V_F}{\partial\langle t\rangle}|_{\tilde\eta} = g(A,B,\beta,\langle c\rangle,F)\times h(\tau\,\langle t\rangle), \tag{3.5}$$

where g is a positive function of its arguments. Since g can be factored out when the first derivative is set to zero, the existence or non-existence of extrema depends only on the properties of h. Notably, this means that, in addition to β and $\langle c\rangle$, the extrema do not depend on A, B or F either. Any changes to A, B and F can be compensated by changing $p\propto\sqrt{A^2+B^2}/F^{2/3}$ to obtain a potential whose first derivative has the same h and, hence, an extremum at the exact same value of $\tau\langle t\rangle$. Importantly, however, note that the scalar expectation value $\langle t\rangle$ depends on the explicit choice of parameter τ.

JHEP07(2024)288

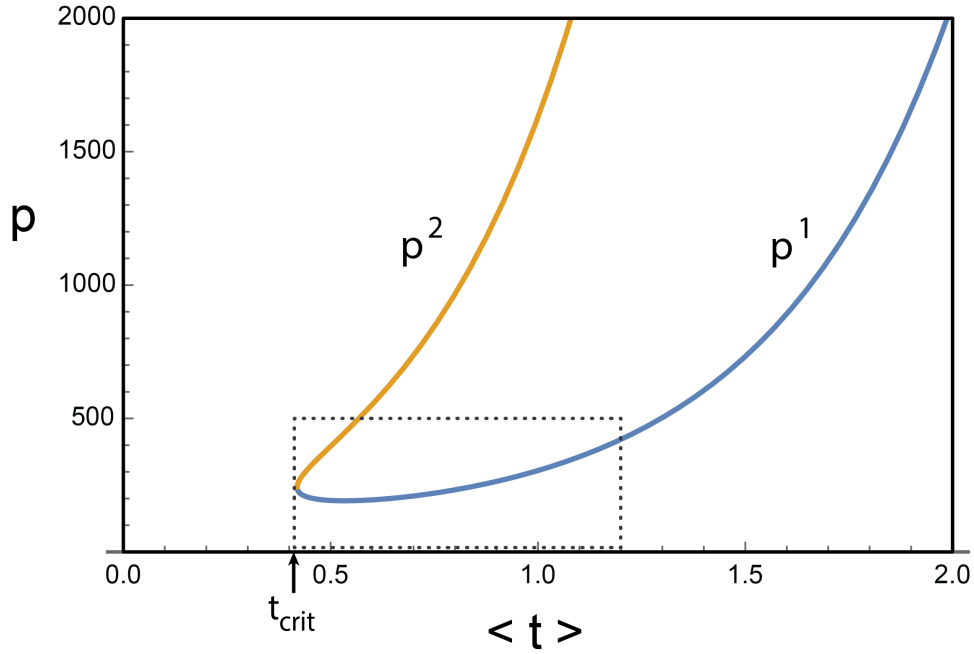

Figure 1. Plot of the two solutions $p^1(\langle t\rangle)$ and $p^2(\langle t\rangle)$ (the blue and gold curves, respectively) as a function of $\langle t\rangle$ for $\tau = 3.0$ and the parameter values given in eq. (3.6). The two semi-infinite curves join together at a point at $\langle t\rangle = t_{\rm crit}$ to form a "combined blue-gold curve." The dotted rectangle shows the region illustrated in the enlargement in figure 2 shown below.

Although they do not affect the existence or locations of extrema, the parameters A, B, β, $\langle c\rangle$, F do affect details like the magnitude of V_F at an extremum and the masses of $\tilde{\phi}$ and $\tilde{\eta}$. For our examples throughout this paper we take, without loss of generality,

$$A = 1/3\,,\ B = A/\sqrt{3}\,,\ \langle c\rangle = 1/\sqrt{3} \text{ and } F = 1.5\,, \tag{3.6}$$

choices that were discussed in ref. [1]. (Note, however, that in discussions below where the range of Pfaffian parameter p is enlarged, parameter F will be allowed to vary). We also chose

$$l = 1 \text{ and } \beta = 6.42 \tag{3.7}$$

for reasons that will be discussed in the next section. Note from (2.4) that for $F = 1.5$ and $l = 1, \beta = 6.42$, the upper bound on $\langle t\rangle$ is given by

$$\langle t\rangle_{bound} = 0.925\,. \tag{3.8}$$

Figure 1 (see also figure 2) is a plot of the *exact* numerical solutions (keeping *all* terms in V_F rather than our approximation) for the roots $p^1(\langle t\rangle)$ and $p^2(\langle t\rangle)$ for $\tau = 3.0$. For $\langle t\rangle < t_{\rm crit}$, the discriminant is negative and $p^{1,2}$ both have unphysical non-zero imaginary parts; so there can be no extrema at $\langle t\rangle < t_{\rm crit}$. For $\langle t\rangle > t_{\rm crit}$, the discriminant is positive and both roots are real. For $\langle t\rangle = t_{\rm crit}$, the discriminant is zero and so the two roots coincide and are real.

JHEP07(2024)288

Draw a vertical line on figure 1 beginning at any value of $\langle t \rangle > t_{\rm crit}$. Clearly, that vertical line will intersect both the gold and blue curves. For there to be an extremum at the chosen value of $\langle t \rangle$, the Pfaffian factor must equal the value of p at one of those two intersections.

Alternatively, for any given p, draw a horizontal line on figure 1 at that value of p and note the intersections with the blue and gold curves. Each corresponds to an extremum of V_F at the value of p and t corresponding to the intersection. By inspection of figure 1, one can see that, depending on the value of p, the horizontal line can have zero, one or two intersections, which means that V_F can have zero, one or two extrema.

5. *Determine which extrema are minima vs. maxima:* by computing the sign of the second derivative $(\partial^2 V_F/\partial\langle t\rangle^2)|_{\tilde{\eta}}$ for the values of p and $\langle t \rangle$ corresponding to the intersections between horizontal lines of constant p and the blue and green curves in figure 1, one can distinguish the extrema.

   It is straightforward to show that any intersections with the *gold* curve correspond to values of p and $\langle t \rangle$ for which $(\partial^2 V_F/\partial\langle t\rangle^2)|_{\tilde{\eta}}$ is positive, that is, a minima of V_F. It is also straightforward to show that V_F at such minima is always negative.

   Intersections with the blue curve are a more complicated story. Intersections with the blue curve correspond to minima of V_F if and only if the slope of the blue curve is negative at the intersection. This is the case only if the value of $\langle t \rangle$ at the extremum lies between $t_{\rm crit}$ and the minimum of the blue curve, which we will label $t_{\rm cross}$ — see figure 2. That is, intersections with the blue curve at $\langle t \rangle < t_{\rm cross}$ correspond to *minima* of V_F. However, intersections with the blue curve at $\langle t \rangle > t_{\rm cross}$ correspond to *maxima* of V_F. An intersection at precisely $\langle t \rangle = t_{\rm cross}$ corresponds to an *inflection point* of V_F.

   If the intersection corresponding to a minimum of V_F lies sufficiently close to $\langle t \rangle = t_{\rm crit}$, the value of V_F is negative; if the intersection lies sufficiently close to $\langle t \rangle = t_{\rm cross}$, the value of V_F is positive. Somewhere in between, there must be a value — which we denote by $t_{V=0}$ — such that, if the intersection lies at $\langle t \rangle = t_{V=0}$, V_F must be zero.

   To summarize: we have explained that, for fixed τ, every intersection between a horizontal line and a blue or gold curve in figure 1 at $(p, \langle t \rangle)$ corresponds to an extremum of V_F for that value of the Pfaffian factor and for that value of $\langle t \rangle$. Intersections with the gold curve always correspond to minima with negative vacuum density V_F. Intersections with the blue curve for which $\langle t \rangle$ lies between $t_{\rm crit}$ and $t_{\rm cross}$ also correspond to minima, but the vacuum density can be negative, zero or positive. Intersections with blue curve for which $\langle t \rangle$ is greater than $t_{\rm cross}$ are maxima.

6. *Classify the possible potential shapes:* figure 2 is an enlargement of figure 1 that can be used to classify the qualitatively different shapes that $V_F(\langle t \rangle)$ can take. We begin with the assumption that there are sufficiently many different compactifications possible that the Pfaffian factor p can take values over a substantial nearly continuous range. A given choice of p lies in one of the three colored bands (from top to bottom: blue, purple, and green) or precisely on the red line dividing the blue and purple bands or precisely

JHEP07(2024)288

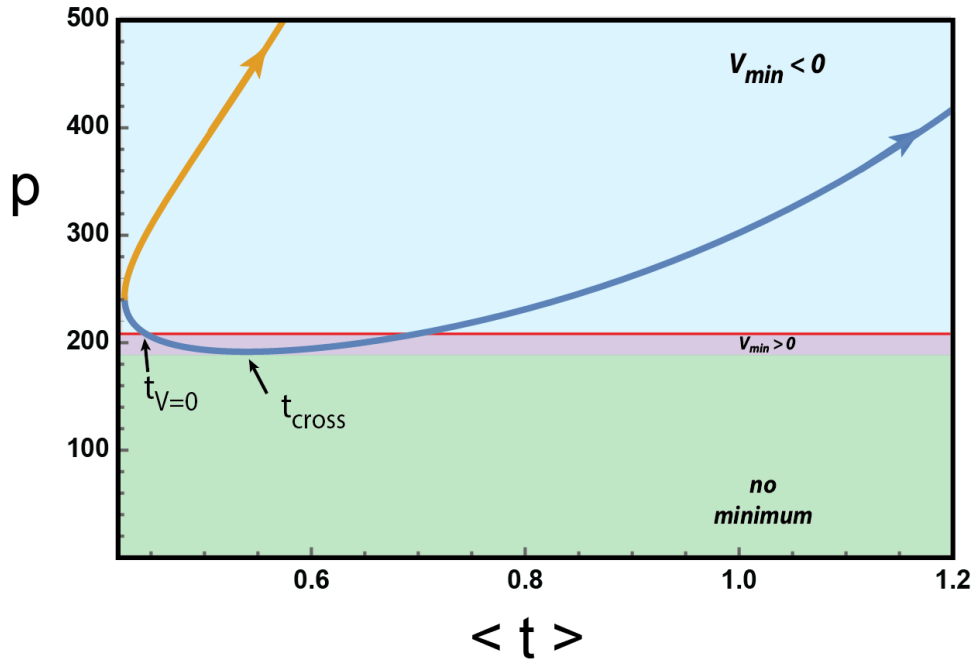

Figure 2. Enlargement of the dotted rectangular region of figure 1 showing the two solutions $p^1(\langle t\rangle)$ and $p^2(\langle t\rangle)$ (the blue and gold curves, respectively) as a function of $\langle t\rangle$ for $\tau = 3.0$ and the parameter values given in eq. (3.6). Note that the abscissa begins on the left at $t_{\rm crit}$, which is equal to 0.42 in this example. The shape of the potential V_F (described as Types 1–5 in the text) depends on the value of the Pfaffian factor p. The shape can be identified by drawing a horizontal line at the given value of p and determining if it lies in the blue shaded region (Type 1); the purple shaded region (Type 2); or in the green shaded region (Type 3). If the horizontal line of constant p lies precisely on the line dividing the purple and green bands, the shape is of Type 4; if the line lies precisely on the red line dividing the blue and purple regions, the shape is of Type 5.

on the line dividing the purple and green bands (which has no special marking). Each of these five possibilities corresponds to a different type of potential shape.

Based on the discussion above of the different extrema, the different shapes take the following forms:

Type 1. The horizontal line lies in the blue shaded region so it intersects the combined blue-gold curve twice. The intersection on the left (at the smaller value of $\langle t\rangle$) is either somewhere on the gold curve or it is on the blue curve with $t_{\rm crit} < \langle t\rangle < t_{V=0}$. In either case, based on the discussion above, the value of $\langle t\rangle$ at the intersection is the location of a minimum of the potential with $V_F < 0$ (negative vacuum density). There is also an intersection at a large value of $\langle t\rangle$ at a point on the blue curve where the slope is positive. Based on the discussion above, this corresponds to a maximum of the potential with $V_F > 0$. A more detailed study of V_F shows that it remains positive at larger values of $\langle t\rangle$ and asymptotes to zero as $\langle t\rangle \to \infty$. The detailed expression for V_F in eq. (2.2) is not precisely accurate beyond $\langle t\rangle = \langle t\rangle_{bound} = \mathcal{O}(1)$ in eq. (2.4), but the asymptotic behavior is correct. The blue curve marked "1" in figure 3 exemplifies the generic shape for cases of Type 1. Note that the negative minimum is a global minimum.

JHEP07(2024)288

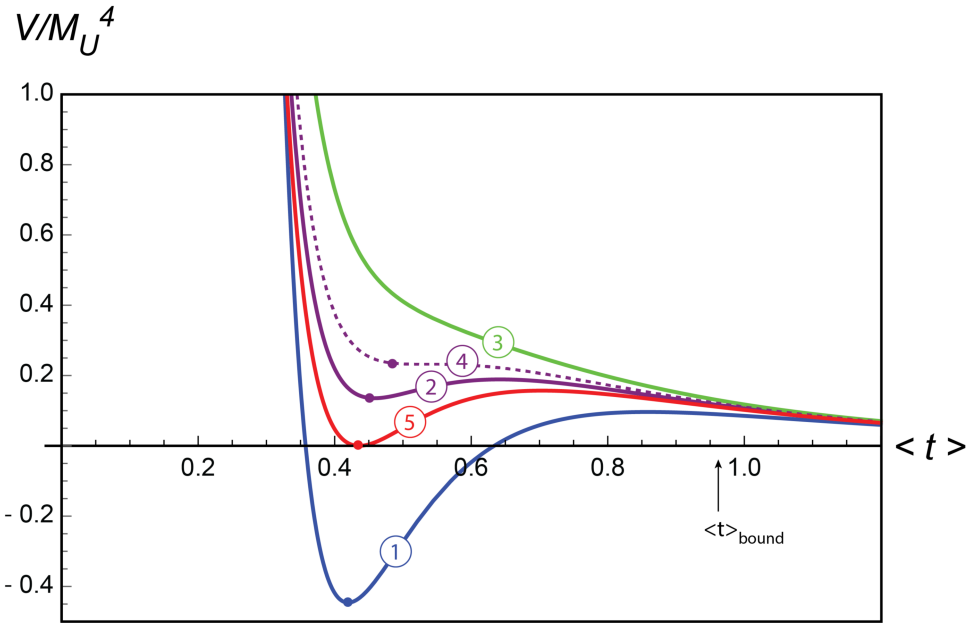

Figure 3. Range of potential shapes corresponding to different values of p for fixed $\tau = 3.0$, and the parameter values given in eqs. (3.6) and (3.7). It follows that $\langle t \rangle_{bound} = .925$. Each potential shape corresponds to drawing a horizontal line of constant p in figure 2, where $p = (250, 200, 175, 192, 210)$ for potential Types 1–5 respectively, as indicated by the numbers inside the circles. The colors of the curves match the colors of the regions in figure 2 in which the horizontal line lies. For example, the blue curve corresponds to $p = 250$ which lies in the blue shaded region of figure 2 and corresponds to Type 1.

Type 2. The horizontal line of constant p lies in the narrow purple shaded region. The horizontal line intersects the blue curve twice, once where the slope is negative at small $\langle t \rangle$ (which corresponds to a minimum) and once where the slope is positive at large $\langle t \rangle$ (which corresponds to a maximum). The minimum occurs at $\langle t \rangle > t_{\rm V=0}$, which means it has positive vacuum density, $V_F > 0$, and is a metastable minimum. The solid purple curve marked "2" in figure 3 exemplifies the generic shape for cases of Type 2.

Type 3. The horizontal line of constant p lies in the green shaded region. It does not intersect either the blue or gold curves, so the potential has no extrema. The green curve marked "3" in figure 3 is a representative of Type 3.
Then there are two special cases which (for fixed τ) occur for unique values of p:

Type 4. The horizontal line of constant p lies on the border between the purple and green shaded regions and passes through $t_{\rm cross}$. The slope of the blue curve at $t_{\rm cross}$ is zero, so corresponds to neither a maximum or minimum of V_F. Instead it corresponds to an inflection point, as illustrated by the dashed purple curve marked "4" in figure 3.

Type 5. The horizontal line of constant p lies on the red line, the border between the blue and purple shaded regions that passes through $t_{V=0}$ where the slope of the blue curve in figure 2 is negative. The negative slope means that value of $\langle t \rangle$ at that intersection corresponds

JHEP07(2024)288

	m_{anom}	m_ϕ	m_η
blue ($V_{\min} < 0$)	1.0×10^{17} GeV	1.7×10^{15} GeV	1.7×10^{15} GeV
red ($V_{\min} = 0$)	9.7×10^{16} GeV	1.2×10^{15} GeV	1.5×10^{15} GeV
purple ($V_{\min} > 0$)	9.0×10^{16} GeV	9.2×10^{14} GeV	1.4×10^{15} GeV

Table 1. The values for m_{anom} and m_ϕ, m_η at the minima of the blue, red and purple curves in figure 3.

to a minimum and the fact that it occurs at $\langle t \rangle = t_{V=0}$ means that vacuum density vanishes, $V_F = 0$. The red line has a second intersection on the right where the slope of the blue curve is positive, corresponding to a maximum. The overall potential shape is the red curve marked "5" in figure 3. In this case, similar to Type 1, the minimum is a global (stable) minimum.

In the examples presented here, with $\tau = 3$ and the other coefficients specified in eqs. (3.6) and (3.7), we have explicitly checked at the minimum of each of the blue, red and purple curves of figure 3 that the following conditions are satisfied; first, $m_{\text{anom}} > M_U = 3.15 \times 10^{16}$ GeV and second, by computing the second derivative of the potential in eq. (2.2), that the masses of the ϕ and η fields are more than an order of magnitude below M_U, consistent with our assumptions in deriving the expression for V_F. See the results in table 1. Ref. [1] gives more examples and includes numerical details about the masses.

Finally, recall from the caption of figure 3 that the potential V_F is calculated for the fixed parameter values given in eqs. (3.6) and (3.7). Specifically note that $F = 1.5$. As mentioned above, it follows from (2.4) that $\langle t \rangle_{bound} = 0.925$. In addition, we have chosen the parameter $\tau = 3$. Each of the five curves shown in figure 3 corresponds to a different value of p. Specifically, the potentials for the curves of Type 1–5 correspond to $p = (250, 200, 175, 192, 210)$ respectively. For concreteness, we limit the discussion here to the curve of Type 5 with $p = 210$; that is, the red curve with minimum at $\langle t \rangle \simeq 4.3$ and $V_F = 0$. The generic results, however, apply to each of the five curves. As discussed in detail in [1], it is important to be able to extend the single value of $p = 210$ to a wide range of values for p, all associated with the red curve with minimum at $\langle t \rangle \simeq 4.3$ and $V_F = 0$.

This extension of the value of p to a wide range of values is important for the following reason. As discussed in our earlier paper [1], other than the fact that the Pfaffian must be some holomorphic polynomial of the associated $B - L$ MSSM heterotic vector bundle moduli, the exact form of this expression is presently unknown. Furthermore, the associated bundle moduli Kähler potential is also unknown. It follows that, at the present time, the vacuum values of these moduli and, therefore, the value of the Pfaffian parameter p cannot be calculated from first principles. Hence, we have simply assumed that parameter p takes the value necessary in order to stabilize the associated moduli–as in figure 3. However, since the value of p cannot at present be explicitly computed, it is a great interest to know if the same moduli stabilization can, in fact, occur over a wide range of p.

As shown in [1], this can be accomplished as follows: recall from section 1, that if one keeps all parameters, including τ, fixed — *but allows F to vary* — then the values of $\langle t \rangle$ at both extrema of the red curve *do not change if one appropriately compensates*

JHEP07(2024)288

by adjusting p. With this in mind, one first notes from figure 3 that the local maximum of the red curve occurs approximately at $\langle t\rangle_{\rm max} = 0.70$. Second, let us increase the value of parameter F from $F = 1.5$ to a value $F_{\rm max}$ such that $\langle t\rangle_{bound} = \langle t\rangle_{\rm max} = 0.70$. Since, $\langle t\rangle_{bound} \propto 1/F^{2/3}$ from (2.4) and the value of $\langle t\rangle_{bound} = 0.925$ for $F = 1.5$, it follows that $F_{\rm max} = 2.28$. Similarly, it was shown above that $p \propto 1/F^{2/3}$. Therefore, when F is increased so that $\langle t\rangle_{bound} = \langle t\rangle_{\rm max} = 0.70$, it follows that the associated Pfaffian parameter decreases to $p = 158$. That is, for the red curve, adjusting F so that $0.70 \leq \langle t\rangle_{bound} \leq 0.925$, the range of parameter p varies over $158 \leq p \leq 210$.

In fact, one can further extend the range of p by going beyond the discussion in [1] as follows. Instead of increasing the value F, let us consider the effect of *decreasing* F. One can show, using the results at the beginning of section 3, that decreasing the value of F will increase the value of the masses of scalar fields ϕ and η at the minima of each of the curves in figure 3, including the red curve. The values of these masses evaluated for $F = 1.5$ are shown in table 1. Note that each mass is more than an order of magnitude smaller than $M_U = 3.15 \times 10^{16}$GeV. Let us now decrease the value of F to $F_{\rm min}$ until at least one of these masses becomes exactly $M_U/10$. We find that this occurs for $F_{\rm min} = 0.8$. It then follows from the above discussion that the value of p *increases* to $p = 320$. We conclude that over the range

$$F_{\rm min} = 0.8 \leq F \leq 2.28 = F_{\rm max} \quad \Longrightarrow \quad 320 \leq p \leq 158\,. \tag{3.9}$$

Therefore, we have shown that the red curve with minimum at $\langle t\rangle \simeq 4.3$ and $V_F = 0$ can be obtained for a greatly increased range of p.

As stated above, all of the examples presented above in figure 3 and table 1 were evaluated using the fixed parameters given in (3.6) and (3.7), as well as taking $\tau = 3$. The value of F in (3.6) was then allowed to vary so as to extend the range of the Pfaffian parameter p. However, it is of interest to ask what happens if, in addition to varying F, one allows the value of τ to vary as well. As above, we will limit our discussion to the red curve with minimum at $V_F = 0$, although similar calculations can be carried out for the blue and purple curves as well. Using the full expression for the V_F potential presented in (2.2), evaluated for the fixed parameters A, B, $\langle c\rangle$ and l, β given in (3.6) and (3.7) respectively, we numerically plot the allowed range for F versus an arbitrary choice of τ. The results are presented in figure 4. Note that the results in (3.9) are shown as the dotted red vertical line at $\tau = 3$. As a second example, it follows from figure 4 that at $\tau = 8$ the allowed values of F are given by

$$F_{\rm min} = 3.7 \leq F \leq 10 = F_{\rm max} \quad \Longrightarrow \quad 115 \leq p \leq 60\,, \tag{3.10}$$

where the range of the Pfaffian parameter p is computed exactly as discussed for the $\tau = 3$ case above.

We conclude that by varying both F and τ over their physically allowed ranges, the value of Pfaffian parameter p that stabilizes the red curve in figure 3 can take values from $p = 60$ and smaller to as large as $p = 320$ and beyond. This greatly improves the likelihood that a future explicit calculation of p will correspond to the stabilized value of the red curve in figure 3–and similarly for the remaining four curves in figure 3.

Finally, we note that since the range of parameter p leading to a specific vacuum (such as the red curve of figure 3) has been shown to be rather large–and higher order perturbative

JHEP07(2024)288

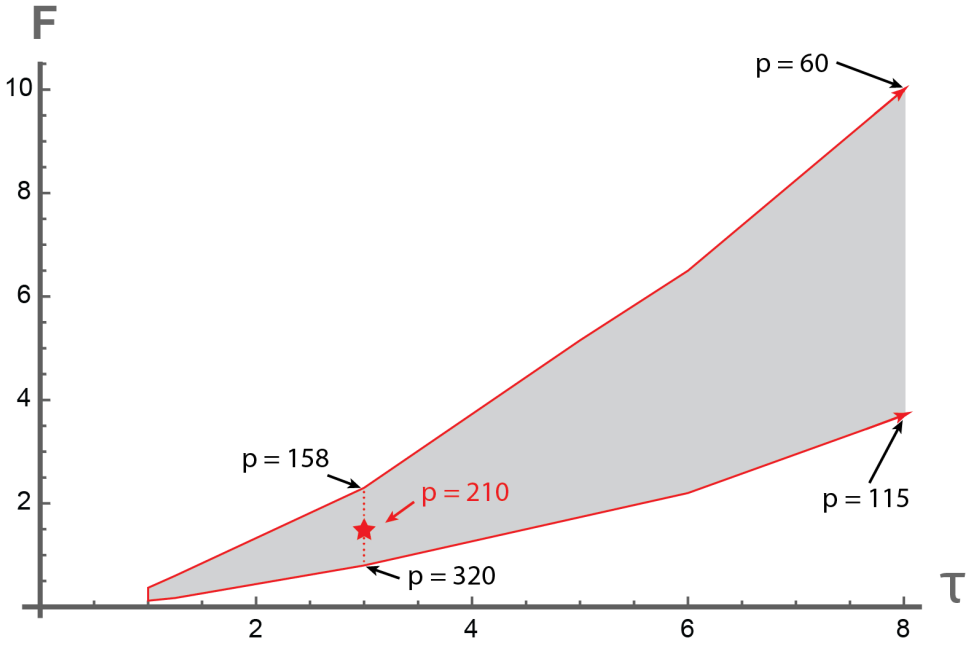

Figure 4. For Type 5 potentials with $V = 0$ at the minimum (that is, the red curve in figure 3), with the A, B, $\langle c \rangle$ and l, β parameters fixed as in (3.6) and (3.7) respectively, the gray region indicates the range of τ and F that satisfies all constraints: namely, $m_{anom} \gtrsim M_U$; the masses of the ϕ and η fields are each at least an order of magnitude less than M_U; and $\langle t \rangle$ at the local maximum of the potential satisfies $\langle t \rangle_{\max} \leq \langle t \rangle_{bound}$. The gray region can be continued to larger values of τ and F, as shown by the red arrows. The red star indicates the Type 5 potential in figure 3 with $\tau = 3$, $F = 1.5$ and $p = 210$. For the same value of τ but different values of F, p can be adjusted so that the minimum of the potential remains at $V = 0$ and at the same value $\langle t \rangle$. For example, in the case of the vertical dashed line at $\tau = 3$, as F changes from 0.8 to 2.3, p ranges from 320 to 158, as indicated in the figure. This shows that a given type of potential can be obtained for a large range of p. As τ increases, the range of F satisfying all constraints also increases. For larger values of F, the value of the Pfaffian parameter is smaller. As a result, the value of p decreases moving up and to the right in the gray region.

corrections due to this supersymmetry breaking should be relatively suppressed, the value of parameter p is expected to be adjustable to account for any perturbative corrections to the potential. Furthermore, since higher order perturbative corrections to potential V should be relatively small, we expect the value of V associated with the adjusted parameter p to remain of the same sign–or very close to the same sign–as in the leading order case.

4 Heterotic $B - L$ MSSM example

What remains is to connect the construction above with a visible sector such that the combination produces realistic particle phenomenology and cosmology. As a concrete example, we have selected the heterotic M-theory $B - L$ MSSM model, using it to define the universal moduli, to give the exact functional form for various parameters and to fix the gauge charge β on the hidden sector. This choice should be viewed as a proof of principle, to show that complete realistic constructions are possible and to explore their observational consequences.

JHEP07(2024)288

This choice has the advantage that its details have been extensively elaborated — see, for example [13, 52, 54, 55].

4.1 The full $h^{1,1} = h^{2,1} = 3$ theory

The heterotic M-theory $B - L$ MSSM theory was developed in a number of papers. Relevant to the present paper is the following. The $B - L$ MSSM vacuum has an observable sector and a hidden sector separated by a fifth-dimension and is compactified on a specific Schoen Calabi-Yau threefold X. This threefold has cohomology $h^{1,1} = h^{2,1} = 3$. Hence, in addition to the dilaton S, there are three real Kähler moduli a^i, $i = 1, 2, 3$, three complex structure moduli z^a, $a = 1, 2, 3$ as well as a real modulus $\hat{R}$ in the fifth dimension.

The three complex structure moduli are defined to be

$$z^a = r^a + ic^a \quad a = 1, 2, 3 \tag{4.1}$$

with the associated Kähler potential

$$\kappa_4^2 \mathcal{K} = -ln[2i(\mathcal{G} - \bar{\mathcal{G}}) - i(z^a - \bar{z^a})(\frac{\partial \mathcal{G}}{\partial z^a} + \frac{\partial \bar{\mathcal{G}}}{\partial \bar{z}^a})] \tag{4.2}$$

where

$$\mathcal{G} = -\frac{1}{6}\tilde{d}_{abc} z^a z^b z^c \tag{4.3}$$

and $\tilde{d}_{abc}$ are the intersection numbers of the specific Shoen threefold X.

The dilaton and the three complex Kähler moduli are define as

$$S = V + i\sigma\,, \quad T^i = t^i + i\chi^i \quad i = 1, 2, 3 \tag{4.4}$$

where

$$V = \frac{1}{6}\tilde{d}_{ijk} a^i a^j a^k, \qquad t^i = \frac{\hat{R}}{V^{1/3}} a^i \tag{4.5}$$

and the associated Kähler potentials are given by

$$\begin{aligned} \kappa_4^2 K_S &= -ln(S + \bar{S}) \\ \kappa_4^2 K_T &= -ln(\frac{1}{48}\tilde{d}_{ijk}(T^i + \bar{T}^i)(T^j + \bar{T}^j)(Tk + \bar{T}^k))\,. \end{aligned} \tag{4.6}$$

The $B - L$ MSSM has a line bundle $L = \mathcal{O}_X(l^1, l^2, l^3)$ with an anomalous U(1) structure group in its hidden sector. It was shown in [47] that under this U(1) transformation the dilaton and Kähler moduli, although carrying no U(1) charge, transform inhomogeneously as

$$\begin{aligned} \delta_\theta S &= i2\pi\epsilon_S^2\epsilon_R^2(-\frac{1}{2}\beta_i^{(2)} l^i)\theta\,, \\ \delta_\theta T^i &= -i2\epsilon_S\epsilon_R^2 l^i\theta\,. \end{aligned} \tag{4.7}$$

Here $\beta_i^{(2)}$ is the gauge charge on the hidden sector. As discussed in [51], the embedding of the U(1) structure group into the hidden sector E_8 has been chosen so that the a coefficient that generically would appear in (4.7) has been set to unity. For specificity, following [51], we henceforth choose the line bundle to be

$$L = \mathcal{O}_X(2, 1, 3)\,, \tag{4.8}$$

JHEP07(2024)288

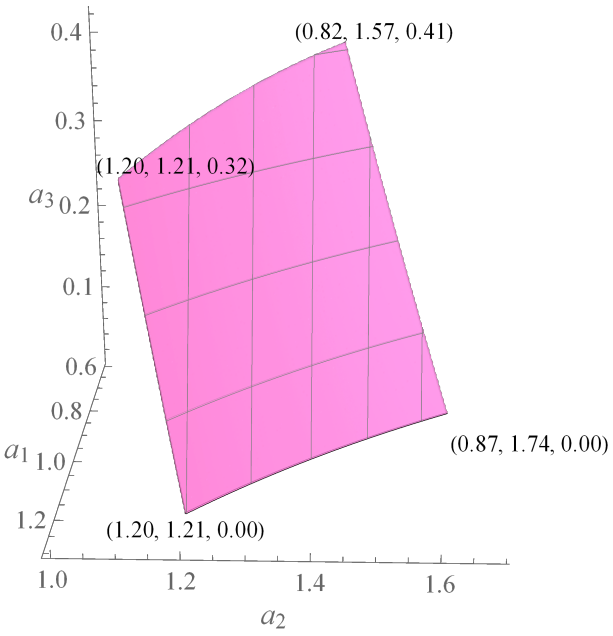

Figure 5. Viable "magenta" region of Kähler moduli space that satisfies all phenomenological and mathematical constraints for the line bundle $L = \mathcal{O}_X(2, 1, 3)$.

although many other line bundles satisfy all constraint conditions. For the specific Schoen Calabi-Yau threefold X and the SU(4) holomorphic vector bundle chosen in the observable sector, it was shown in [51], absorbing the five-brane class into the hidden sector, that

$$-\beta_i^{(2)} = \beta_i^{(1)} = (\frac{2}{3}, -\frac{1}{2}, 4)\,. \tag{4.9}$$

Combining (4.8) and (4.9), it follows that the $-\frac{1}{2}\beta_i^{(2)} l^i$ factor in (4.7) is given by

$$-\frac{1}{2}\beta_i^{(2)} l^i = 6.42\,. \tag{4.10}$$

Finally, within the context of this $h^{1,1} = h^{2,1} = 3$, $B - L$ MSSM theory, it was shown in [51] that all mathematical and phenomenological constraints are satisfied by a well-defined, but constrained, subspace of the three-dimensional real Kähler moduli space. Choosing a specific gauge, called unity gauge, defined by

$$\frac{\epsilon_S' \hat{R}}{V^{1/3}} = 1\,, \tag{4.11}$$

it was found that all constraints will be satisfied for real Kähler moduli in the so-called "magenta" surface shown in figure 5.

Scanning over this surface and using V in (4.5), we find that the real scalar field $s = V$ is confined to the range

$$s \in [0.55, 1.22]\,. \tag{4.12}$$

It follows from definition (4.11) of unity gauge, that

$$\hat{R} = \frac{s^{1/3}}{\epsilon_S'}\,. \tag{4.13}$$

JHEP07(2024)288

Using the result in [1] that

$$\epsilon'_S = 0.690 F^{4/3}\,, \tag{4.14}$$

where F is a free real parameter in the range $0.6 \lesssim F \lesssim 2$, it follows that the real field $\hat{R}$ is confined to the range

$$\hat{R} \in [\frac{1.19}{F^{4/3}}, \frac{1.55ß}{F^{4/3}}]\,. \tag{4.15}$$

4.2 Reduction to the universal complex structure and Kähler moduli

In order to use the $h^{1,1} = h^{2,1} = 1$ results of the previous sections within the context of the $B - L$ MSSM, it is necessary to restrict the analysis to the "universal" complex structure and Kähler moduli, which are defined as follows.

Recall that the Kähler potential for the three complex structure moduli z^a,$a = 1, 2, 3$ is given by (4.2) with

$$\mathcal{G} = -\frac{1}{6}\tilde{d}_{abc} z^a z^b z^c\,. \tag{4.16}$$

The universal complex structure modulus z is defined by setting

$$\tilde{d} z^3 = \frac{1}{6}\tilde{d}_{abc} z^a z^b z^c \tag{4.17}$$

for an arbitrary integer $\tilde{d}$. It follows that

$$\mathcal{G} = -\tilde{d} z^3 \tag{4.18}$$

and, hence, for the universal complex structure modulus

$$\kappa_4^2 \mathcal{K} = -ln[i\tilde{d}(z - \bar{z})^3]\,, \tag{4.19}$$

where

$$z = r + ic\,. \tag{4.20}$$

Similarly, recall from (4.6) that the Kähler potential for the three Kähler moduli T^i, $i = 1, 2, 3$ is given by

$$\kappa_4^2 K_T = -ln(\frac{1}{48}\tilde{d}_{ijk}(T^i + \bar{T}^i)(T^j + \bar{T}^j)(T^k + \bar{T}^k)) \tag{4.21}$$

Using the results in (4.5), it follows that this Kähler potential can be re-written as

$$\kappa_4^2 K_T = -3ln(\hat{R})\,. \tag{4.22}$$

Therefore, we should define the universal modulus T to be such that

$$\kappa_4^2 K_T = -3ln(T + \bar{T}) = -3ln(\hat{R}) \tag{4.23}$$

and, hence, that

$$T = t + i\chi\,, \quad t = \frac{\hat{R}}{2}\,. \tag{4.24}$$

JHEP07(2024)288

Note that the definition of unity gauge in (4.13) now becomes

$$t = \frac{s^{1/3}}{2\epsilon_S'} \,. \tag{4.25}$$

Also, it follows from (4.15) that t along the magenta surface is restricted to lie in the range

$$t \in [\frac{0.594}{F^{4/3}}, \frac{0.774}{F^{4/3}}] \,. \tag{4.26}$$

Now let us compare the anomalous inhomogeneous transformation of S in the $h^{1,1} = h^{2,1} = 3$ case given in (4.7) with the same transformation of S in the $h^{1,1} = h^{2,1} = 1$ case presented in [1, 48] and given by

$$\delta_\theta S = i2\pi\epsilon_S^2\epsilon_R^2(\beta l)\theta \,, \tag{4.27}$$

where $L = \mathcal{O}(l)$ defines a "universal" line bundle. Using (4.10), this leads to the identification that

$$-\frac{1}{2}\beta_i^{(2)} l^i = \beta l = 6.42 \,. \tag{4.28}$$

With these definitions of the universal complex structure and Kähler moduli, as well as the definition of the dilaton S given in (4.4), we can now apply all the results in [1] — and outlined in the previous sections — to the $B - L$ MSSM vacuum.

It is of interest to know whether any of the points on the magenta surface also satisfy the condition that $FI = 0$. As shown in ref. [1], $FI = 0$ if and only if

$$s = \frac{\epsilon_S'\beta}{3} t = 0.230 F^{4/3}\beta \; t \,. \tag{4.29}$$

Combining this with the unity gauge definition (4.25), we find that there is a unique point — which we denote with a hat — that is both on the "magenta" surface and satisfies the $FI = 0$ condition. It is given by

$$\hat{s} = 0.068\beta^{3/2} \,, \quad \hat{t} = \frac{0.296}{F^{4/3}}\beta^{1/2} \,. \tag{4.30}$$

Comparing $\hat{s}$ to the allowed range for s given in (4.12), we find that, for the "magenta" surface to be consistent with $FI = 0$, the coefficient β must lie in the range

$$4.03 \leq \beta \leq 6.85 \,. \tag{4.31}$$

It is clear from (4.28) that this will be the case only if one takes

$$l = 1 \,, \quad \beta = 6.42 \,. \tag{4.32}$$

Therefore, the point in the "magenta" surface that simultaneously satisfies the D-flatness condition $FI = 0$ is given by

$$\begin{aligned} \hat{s} &= .068(6.42)^{3/2} = 1.11 \; (\in [0.55, 1.22]) \,, \\ \hat{t} &= \frac{0.296(6.42)^{1/2}}{F^{4/3}} = \frac{0.749}{F^{4/3}} \; (\in (\frac{0.594}{F^{4/3}}, \frac{0.774}{F^{4/3}}]) \,. \end{aligned} \tag{4.33}$$

Note that $\hat{s}$ and $\hat{t}$ are in the allowed range for any choice of F. We will refer to the geometric moduli $\hat{s}$, $\hat{t}$ as the "physical point".

JHEP07(2024)288

	m_{anom}	m_ϕ	m_η
blue ($V_{\min} < 0$)	9.7×10^{16} GeV	1.54×10^{15} GeV	1.6×10^{15} GeV
red ($V_{\min} = 0$)	9.7×10^{16} GeV	1.3×10^{15} GeV	1.6×10^{15} GeV
purple ($V_{\min} > 0$)	9.7×10^{16} GeV	1.3×10^{14} GeV	1.6×10^{15} GeV

Table 2. The values for m_{anom} and m_ϕ, m_η at the minima of the blue, red and purple curves in figure 6.

4.3 Stabilizing the universal geometric moduli at the physical point

Now we come to the crucial question: can the $B-L$ MSSM theory described in this section have a moduli potential with stable or metastable minima, as described in the previous section, such that the resulting vacua produce realistic particle phenomenology? The challenge is that the $B-L$ MSSM theory imposes additional constraints.

As we have explained, in the $B-L$ MSSM, once one has chosen to work in unity gauge (4.25), there is a limited "magenta" region in Kähler moduli space that satisfies all mathematical and phenomenological constraints. Furthermore, within that limited region, there is a unique point that is also consistent with the requirement that the Fayet-Iliopoulos term $FI = 0$. Given the fact that the $B-L$ MSSM requires that $l = 1$ and $\beta = 6.42$, it follows from (4.33) that the vacuum must be located at $\langle t \rangle = \hat{t} = \frac{0.749}{F^{4/3}}$, where thus far we have limited parameter F to the range $.6 \lesssim F \lesssim 2$. We note that in all examples in the previous section, we chose $l = 1$ and $\beta = 6.42$ — see (3.7) — knowing that this would be necessary in the $B-L$ MSSM example. However, in the sequence of potentials shown in figure 3, the minima were marked with small colored dots to make it apparent that they occurred at different values of $\langle t \rangle$, so at most one of the minima could lie at $\langle t \rangle = \hat{t}$. In fact, for the parameters chosen for figure 3, specifically $F = 1.5$, none of them did.

However, previously we fixed all parameters except for *one*, p, which was allowed to vary. This limited our flexibility. Our question now becomes: is it possible to keep all parameters fixed (including F) except for *two*, τ and p, and to adjust these two so that the minima for each of the three types of potentials with stable or metastable minima (Types 1, 2 and 5) occur at exactly the same value of $\langle t \rangle$, namely at $\langle t \rangle = \hat{t} = \frac{0.749}{F^{4/3}}$, as required for consistent particle phenomenology, and $FI = 0$ (recall that potential Types 3 and 4 have no minima). Figure 6 demonstrates that the answer is yes.

For the analysis associated with figure 6, we once again choose the same parameters as those used in figure 1 — that is, the coefficients given in (3.6) and (3.7). We emphasize that in (3.6), the parameter F is chosen to be $F = 1.5$. It then follows from (2.4) that $\langle t \rangle_{bound} = 0.925$ and from (4.33) that $\hat{t} = 0.436$. In figure 6, the potential V_F is plotted as a function of $\langle t \rangle$ for various choices of (τ, p), with the allowed range restricted to $0 \leq \langle t \rangle \leq 0.925$. Once again, there are potentials whose minima have negative, zero or positive vacuum energy density. This time, however, the minima all occur at $\langle t \rangle = \hat{t} = 0.436$, proving that including all of the $B-L$ MSSM constraints does not rule out any of the three categories of minima.

As discussed in [1], it is essential to compute the masses of the scalar fluctuations ϕ and η at the minima of each curve in figure 6, and to show that they are substantially smaller than the compactification scale $M_U = 3.15 \times 10^{16}$ GeV. The results of these calculations for

JHEP07(2024)288

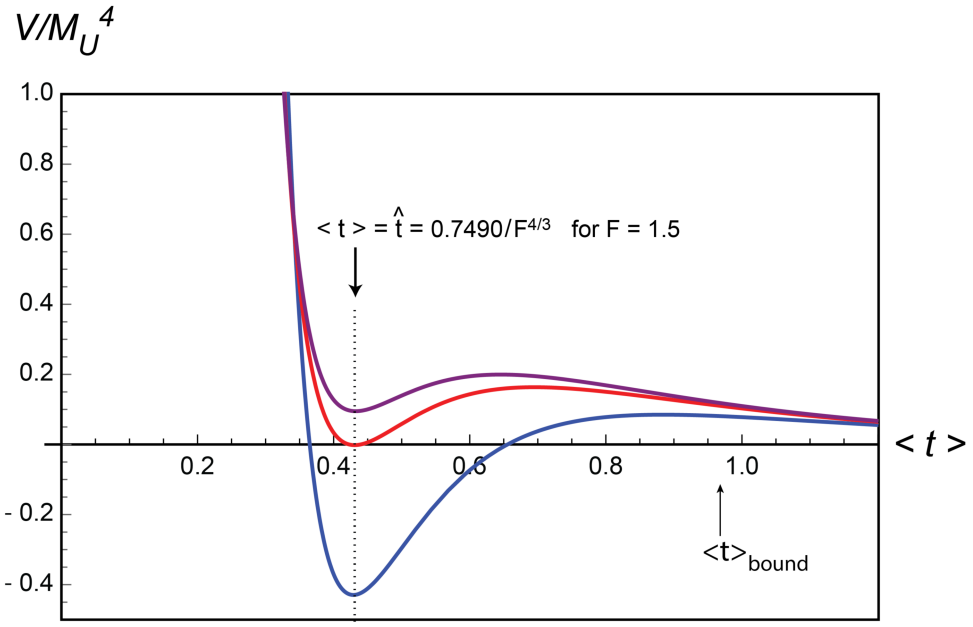

Figure 6. Examples of potentials whose minima have negative vacuum energy density (blue curve, Type 1), positive vacuum energy density (purple curve, Type 2) and zero vacuum energy density (red curve, Type 5) and which all satisfy the $B-L$ MSSM "magenta" and the $FI=0$ constraint $\langle t\rangle = \hat{t} = \frac{0.749}{F^{4/3}} = 0.436$ at their minima. For this figure, we chose all parameters to be those given in (3.6) and (3.7) for each of the three potentials — leaving two free parameters, τ and p. Both τ and p were varied to keep the minima at $\langle t\rangle = \hat{t}$ in all three cases, which ensures consistent particle phenomenology and $FI=0$ at each vacuum of the stabilized moduli. Specifically, the values of τ and p are: $(\tau = 2.93,\, p = 252)$ for Type 1; $(\tau = 3.1,\, p = 204)$ for Type 2; and $(\tau = 3.03,\, p = 210)$ for Type 5.

the blue, red and purple curves, as well as the value of the m_{anom}, at $\hat{t} = .436$ are shown in table 2. For each of the three curves, the masses of ϕ and η are substantially below M_U and, hence, they are included in the low energy effective theory.

4.4 Enhancing the range of Pfaffian parameter p

As presented in the caption of figure 6, for a given value of τ, each curve has its shape, and, hence, its extrema determined by a fixed value of p. For example, the red curve has $\tau = 3.03$ with a fixed value of $p = 210$. As discussed in detail in section 6 of [1], it is of importance, for any specific curve, to be able to extend the range over which the Pfaffian parameter p can vary. This increases the probability that this Pfaffian minimizes the effective potential energy of the vector bundle moduli. A concrete method for doing this was presented in [1] and used at the end of section 3 — which we now apply to the three curves in figure 6. For specificity, let us begin by considering the red (Type 5) curve — whose minumum has vanishing potential energy. As shown in section 1 above, if one keeps all parameters, including τ, fixed — *but allows F to vary* — then the $\langle t\rangle$ locations of both extrema of the red curve do not change if one appropriately compensates by adjusting p. Importantly, it was shown in section 6 of [1] that for the class of heterotic M-theories we are discussing — and, in

JHEP07(2024)288

particular, the $B-L$ MSSM — the value of parameter F becomes arbitrary and need not be confined to the range $0.6 \lesssim F \lesssim 2$.

With this in mind, we proceed by reiterating part of the discussion at the end of section 3 — limiting our analysis in this section, for simplicity, to the results of increasing the value of F only. First, determine the $\langle t \rangle$ value of the local *maximum* of the red curve, which we find from figure 6 to be $\langle t \rangle_{\rm max} = 0.70$. Second, we increase the value of parameter F from $F = 1.5$ to a value $F_{\rm max}$ such that $\langle t \rangle_{bound} = \langle t \rangle_{\rm max} = 0.70$. Since, from (2.4) $\langle t \rangle_{bound} \propto 1/F^{2/3}$, and the value of $\langle t \rangle_{bound} = 0.925$ for $F = 1.5$, it follows that $F_{\rm max} = 2.28$. Similarly, it was shown above that $p \propto 1/F^{2/3}$. Therefore, when F is increased so that $\langle t \rangle_{bound} = \langle t \rangle_{\rm max} = 0.70$, it follows that the associated Pfaffian parameter decreases to $p = 159$. That is, for the red curve, adjusting F so that $0.70 \leq \langle t \rangle_{bound} \leq 0.925$, the range of parameter p varies over $159 \leq p \leq 210$.

This analysis is identical to that discussed in section 6 of [1]. However, when applied to the $B-L$ MSSM vacuum there is another important constraint that must be satisfied: as mentioned above, when raising the value of parameter F from $F = 1.5$ to $F_{\rm max} = 2.278$ and adjusting p from $p = 210$ down to $p = 159$, the location of the minimum of the red curve remains at $\langle t \rangle = 0.436$. However, using (4.33), it follows that the value of $\hat{t}$ decreases from 0.436 for $F = 1.5$ down to $\hat{t} = 0.249$ for $F_{\rm max} = 2.278$. That is, the value of $\langle t \rangle$ at the unique point in the magenta surface satisfying $FI = 0$ has become smaller and no longer lies at the minimum of the red curve. It would appear, therefore, that the vacuum of the red curve no longer satisfies the necessary physical constraints with $FI = 0$. However, as we now show, this is not the case.

As discussed above, within the context of this $h^{1,1} = h^{2,1} = 3$, $B-L$ MSSM theory, it was shown in [53] that all mathematical and phenomenological constraints are satisfied by a well-defined, but constrained, subspace of the three-dimensional real Kähler moduli space. As analyzed in [53], all of these constraints remain invariant under a scaling of the Kähler and $\hat{R}$ moduli given by

$$a^i \longrightarrow \mu a^i, i = 1, 2, 3 \quad \text{and} \quad \hat{R} \longrightarrow \mu^3 \hat{R}\,. \tag{4.34}$$

In [53], as used in the discussion thus far in this paper, it was most convenient to solve all the mathematical and physical constraints by using the scaling in (4.34) to choose a specific moduli gauge, called "unity gauge", defined by

$$\frac{\epsilon_S' \hat{R}}{V^{1/3}} = 1\,. \tag{4.35}$$

Working in this gauge, we found that all constraints will be satisfied for the real Kähler moduli in the so-called "magenta" surface shown in figure 5. Within this choice of gauge, we showed above that there is a unique value for the "universal" real Kähler modulus t defined in (4.24), namely $\hat{t} = \frac{.7490}{F^{4/3}}$, which is on this magenta surface and simultaneously satisfies the $FI = 0$ constraint. For $F = 1.5$, this led to the minima of the three curves in figure 6 being located at .436. However, we note that this value for $\hat{t}$ is highly dependent on the fact that we chose to work in a specific moduli gauge, namely unity gauge. However, the solution to all the mathematical and physical constraints will remain valid for any choice of gauge;

JHEP07(2024)288

that is, for any scaling with non-zero real parameter μ of the Kähler and $\hat{R}$ parameters as given in (4.34). For a fixed value of μ, expression (4.35) becomes

$$\frac{\epsilon_S' \hat{R}}{V^{1/3}} = \mu^2 \tag{4.36}$$

and one will obtain a new surface in Kähler moduli space — a linear scaling of the "magenta" region shown in figure 5 — for which all constraints are also satisfied. One can now ask: what is the value of $\langle t \rangle$ that lies on this new scaled surface and simultaneously satisfies $FI = 0$? It is clear from the analysis leading to (4.33) that this new value of $\langle t \rangle$ is given by

$$\hat{\hat{t}} = \frac{0.749}{F^{4/3}} \mu^3 \,, \tag{4.37}$$

where the double hat indicates that this is in a new moduli gauge specified by μ. Choosing the gauge parameter μ to be

$$\mu = 1.20 \tag{4.38}$$

and recalling that $F_{\text{max}} = 2.28$, it follows that

$$\hat{\hat{t}} = \frac{0.749}{F_{\text{max}}^{4/3}} \mu^3 = 0.436 \,. \tag{4.39}$$

Hence, we have shown that the minimum of the red curve in figure 6 indeed satisfies all mathematical and phenomenological constraints as well as $FI = 0$. To summarize: for the red curve, with a minimum with zero potential energy and parameter $\tau = 3.03$, we find that $F_{\text{max}} = 2.28$. Over the range of F from F_{max} to $F = 1.5$, it follows that

$$0.70 \leq \langle t \rangle_{bound} \leq 0.925. \quad \Longrightarrow \quad 158 \leq p \leq 210 \,. \tag{4.40}$$

Furthermore, by appropriately choosing the moduli gauge parameter, the minimum of the potential satisfies the $FI = 0$ constraint for any value of F in this allowed range.

Suffice it to say that a similar analysis will also extend the range of the Pfaffian parameter p for both the blue and purple curves in figure 6. Here, we simply state the results. For the blue curve, with a minimum with negative vacuum potential energy and parameter $\tau = 2.93$, we find we find that $F_{\text{max}} = 1.56$. Over the range of F from F_{max} to $F = 1.5$, it follows that

$$0.90 \leq \langle t \rangle_{bound} \leq 0.925 \quad \Longrightarrow \quad 245 \leq p \leq 252 \,. \tag{4.41}$$

Applying the same analysis to the purple curve, with positive vacuum potential energy with parameter $\tau = 3.1$, we find that $F_{\text{max}} = 2.546$. Over the range of F from F_{max} to $F = 1.5$, it follows that

$$0.65 \leq \langle t \rangle_{bound} \leq 0.925 \quad \Longrightarrow \quad 101 \leq p \leq 204 \,. \tag{4.42}$$

Finally, as for the red curve, by appropriately choosing the moduli gauge parameter, the minimum of the potential of the blue and purple curves satisfies the $FI = 0$ constraint for any value of F in their allowed ranges.

JHEP07(2024)288

5 Implications for cosmology and fundamental physics

The key results of the preceding analysis (including ref. [1]) are that:

- five types of potential shapes are possible for the moduli sector (as illustrated in figure 3);
- three of them (Types 1, 2 and 5) have minima corresponding to either stable or long-lived metastable vacuum states; and
- a visible sector with particle phenomenology in agreement with all current observations (for example, the $B-L$ MSSM) can be incorporated.

In this section, we first discuss whether the observational constraints imposed by ΛCDM cosmology can be satisfied by these M-theoretic models and comment briefly on the implications for axion-based cosmology. We then consider whether these models satisfy the Swampland conjectures [2–6] that are proposed to apply to string theory or quantum gravity, generally. Finally, we discuss the consistency conditions that must be satisfied by theories with extra dimensions and the metrics assumed in the M-theoretic models [24–26].

5.1 Consistency with ΛCDM cosmology

Of the five types of potentials, only Type 5 is compatible with ΛCDM cosmology.

Type 1 potentials have a global minimum with very negative vacuum energy, $\langle V\rangle = -\mathcal{O}(M_U^4)$, a strongly anti-deSitter ground state that is inconsistent with observations. Type 2 potentials have a local minimum with large positive vacuum energy density, $\langle V\rangle = +\mathcal{O}(M_U^4)$, which is also incompatible with ΛCDM. A universe with $\langle t\rangle$ trapped in a Type 2 minimum would undergo inflation, but there would be no path to a graceful exit — for example, through "slow roll." Bubble nucleation would be required to escape, and the escape would be to large values of $\langle t\rangle$ where supersymmetry is restored and the particle phenomenology is inconsistent with observations. Types 3 and 4 have no local or global minima at all, so there is no stopping a rapid escape to large values of $\langle t\rangle$ in these cases as well.

On the other hand, Type 5, with a globally stable minimum at $\langle V\rangle \approx 0$, can be made to fit all current cosmological observations. The minimum is globally stable for $\langle V\rangle \lesssim 0$ and very long-lived for $\langle V\rangle \gtrsim 0$. In the latter case, the barrier height is $\mathcal{O}(M_U^4)$, so bubble nucleation is highly suppressed such that the lifetime of the metastable phase exponentially exceeds a Hubble time.

In the analysis here, we have not included contributions to the vacuum density due to the electroweak symmetry breaking phase transition — associated with the Higgs field — or any other contributions with energy densities much less than M_U. In principle, though, these can be easily accommodated by tiny changes in parameters that can shift the total vacuum density to equal zero without significantly changing the shape of the Type 5 potential.

To incorporate dark energy, there are at least two options. First, the parameter changes described above can be finely adjusted to shift the vacuum density above zero so that the total is slightly positive and equal to the observed dark energy density. The small positive shift would transform the vacuum from being globally stable to a very long-lived metastable state (which eventually would tunnel to the $V \to 0$, $\langle t\rangle \to \infty$ state).

JHEP07(2024)288

Alternatively, it is possible to modify Type 5 models to incorporate Quintessence Cold Dark Matter (QCDM) rather than ΛCDM cosmology. Dark energy can be included by introducing a low energy density quintessence-like scalar field that adds a degree of freedom to the potential along some additional field direction out of the plane of the plot of the potential in figure 6. The quintessence field could be rolling slowly towards the true vacuum with $V = 0$ along this additional direction, so that the universe eventually settles in the $V = 0$ ground state. In this situation, there is the novel possibility that $\langle t \rangle$ is prevented from ever escaping to infinity, so that supersymmetry is never restored and extra dimensions never open up. Natural candidates for the quintessence field are the Kähler moduli or associated axions that would be added if the cohomology were extended to $h^{1,1} > 1$ (see the discussion of axions below).

It should be noted, though, that Type 5 models only occur for a limited range of parameters. In figure 2, where fixed values of A, B and F are assumed, this corresponds to constraining the Pfaffian parameter p to be exponentially close to the horizontal red line. However, as we have noted in the discussion of eq. (3.5), a combination of variations in A, B and F compensated by a changing $p \propto \sqrt{A^2 + B^2}/F^{2/3}$ enables a rather wide range of p that maintains the same potential type, as exemplified by the example described by eq. (4.40). Variations from unity gauge enable a yet wider range. Hence, there is actually a reasonable chance of finding a vector bundle moduli sector that can produce p in the range required to obtain a Type 5 potential.

5.2 Implications for axions and axion-like particles

Our construction has implications for cosmological models of inflation, dark energy and dark matter based on axion-like fields derived from string theory, such as η. A common approximation is to treat the axion potential as a single cosine potential with a constant coefficient or, in the case of axiverse models involving many axions, a sum of such terms.

Our example, though, shows that the potential for axion-like fields in string theory is generically more complicated. This is even true for the simplest cohomology, as considered in this paper, where $h^{1,1} = h^{2,1} = 1$ and there is only a single axion-like field, η. We found that the potential V_F contains three different terms with cosine factors whose arguments each include η. Also, the coefficients are not constants. Rather, they are different complicated functions of other fields. In axion-based cosmological models in which the axion is evolving with time (e.g., models of inflation or quintessence dark energy), these interactions would induce back-reactions from the fields to which they are coupled which may lead to additional observational constraints.

For more realistic examples like the $B - L$ MSSM theory, the axion story is more complicated. For example, a full implementation requires a Schoen Calabi-Yau threefold X with cohomology $h^{1,1} = h^{2,1} = 3$ that leads to three axion-like fields. The resulting supergravity potential includes more complicated coefficients and many kinds of cross terms. These are functions of different combinations of axion fields multiplied by coefficients involving the dilaton and Kähler moduli.

A proper analysis for axion cosmology derived from string theory will require considering potential energy landscapes of this more complex type, which is a challenge to analyze. But this may also offer opportunities, such as novel phenomena not found in the usual simplistic approximations. This will be a target for our future research.

JHEP07(2024)288

5.3 Conjectured constraints from string theory and quantum gravity

The potentials for heterotic M-theory presented in this paper are interesting test cases for the Swampland conjectures [2–6] that are postulated to be satisfied by string theory and any consistent theory of quantum gravity. Here we consider the Transplanckian Censorship Conjecture (TCC) [2] bounds in the asymptotic regime of large moduli field for all potentials and in the center of moduli space for monotonic potentials because the TCC conjectures are well-established in the sense that the constraints can be derived by independent arguments [56, 57].

The TCC [2] implies that, for *large* values of moduli fields (transformed so that their kinetic energies are canonically normalized), there is a positive lower bound on the gradient of the total potential if $V > 0$, namely

$$\frac{|\nabla V|}{V} \geq \frac{2}{\sqrt{d-2}}, \tag{5.1}$$

where d is the spacetime dimension and ∇ is the derivative with respect to the canonically normalized field Φ (see below). Since $d = 4$ in our case, the Swampland lower bound is equal to $\sqrt{2}$.

In ref. [1], we showed that all five types of potentials presented in this paper approach zero from above; that is, for large $\langle t\rangle$, $V > 0$, but $V \to 0$ as $\langle t\rangle \to \infty$ and, in addition, they all satisfy the bound in (5.1). In brief, we pointed out that V in the large $\langle t\rangle$ limit is dominated by the first term in the square brackets in eq. (2.2), the only one of the six terms that is not suppressed by a factor of the form $e^{-\alpha\langle t\rangle}$. In this limit, $V \propto 1/\langle t\rangle^4$. However, the kinetic energy density for $\langle t\rangle$ is non-canonical, $\frac{3}{4}\frac{(\partial\langle t\rangle)^2}{\langle t\rangle^2}$. To convert to a canonically normalized kinetic energy, we rewrite $\langle t\rangle$ in terms of a new scalar real scalar field Φ as $\exp\left(\sqrt{2/3}\Phi\right)$. The potential $V \propto 1/\langle t\rangle^4$ then becomes $V \propto \exp[-4\sqrt{2/3}\Phi]$. From this we find

$$\frac{|dV/d\Phi|}{V} = 4\sqrt{2/3} > \sqrt{2}, \tag{5.2}$$

which satisfies the TCC and Strong deSitter Conjecture, eq. (5.1).

The Swampland conjectures are more subtle near the *center of moduli space* — for example, for $\langle t\rangle = \mathcal{O}(1)$. This is of interest, since this is the region where the extrema of our potentials are located. For *monotonically decreasing potentials only*, there is a TCC constraint on the slope. *Violation* of this slope constraint requires that

$$\frac{|\nabla V|}{V} \leq \frac{2}{\sqrt{(d-1)(d-2)}} \tag{5.3}$$

over a field range

$$\Delta\Phi \geq \frac{\sqrt{(d-1)(d-2)}}{2} \ln\left(\frac{(d-1)(d-2)}{2\,V_{\rm max}}\right), \tag{5.4}$$

where $V_{\rm max}$ is the maximum value of V within the field range (expressed in reduced Planck units) and Φ has canonical kinetic energy density [2]. The monotonic potentials in our study correspond to Type 3 (no extremum) and Type 4 (an inflection point), as illustrated in figure 3. For these cases, the value of $V_{\rm max}$ is $\mathcal{O}(M_U^4) \approx 10^{-8}$ and $d = 4$. Using these

JHEP07(2024)288

values, violating the TCC bound requires having $\frac{|\nabla V|}{V} \leq \sqrt{2/3}$ (eq. (5.3)) over a field range $\Delta\Phi > 20$ (eq. (5.4)). In our Type 4 examples where $\nabla V = 0$ at the inflection point, the range is $\Delta\Phi \approx 0.5$, far less than required for a TCC violation. (As a further check, one can also show that $|M_P^3 \nabla^3 V/V| \gg 1$ at the inflection point, which is too large to support significant accelerated expansion; see appendix B in [2].) Since Type 3 potentials are steeper than Type 4, the range is even smaller, so they do not violate the TCC either. For Types 1, 2 and 5, which have minima in the center of moduli space, there is currently no accepted Swampland conjecture. We therefore conclude the following:

- *All the heterotic M-theory potentials presented here and in ref. [1] satisfy currently well-established Swampland conjectures.*

There are, however, other conditions specific to heterotic M-theory that need to be checked; namely, in order to be safely below the strongly coupled limit, it is necessary that

$$\mathbb{L} M_{11} \gg 1 \qquad \text{and} \qquad \mathbb{V}_{CY}^{1/6} M_{11} \gg 1 \tag{5.5}$$

where M_{11} is the 11d Planck mass, $\mathbb{V}_{CY} = vs$ is the physical 6d Calabi-Yau volume and $\mathbb{L} = 2\pi\rho t$ is the physical length of the compact heterotic dimension. To convert these bounds into constraints involving the 4d Planck mass M_P, one can use the relation

$$M_{11}^9 v(\pi\rho) \approx M_P^2, \tag{5.6}$$

assuming s and t are $\mathcal{O}(1)$ in reduced Planck units. Furthermore, using the results from [1] that $\pi\rho = 5Fv^{1/6}$, $M_P = 1.22 \times 10^{19}$GeV and $M_U = 3.15 \times 10^{16}$GeV, as well as equation (4.29), it follows that the relations in eq. (5.5) then reduce to

$$1 \ll \mathbb{L} M_{11} = 38.8\, F^{\frac{8}{9}} t \tag{5.7}$$

and

$$1 \ll \mathbb{V}_{CY}^{\frac{1}{6}} M_{11} = 3.04\, \beta^{\frac{1}{6}} F^{\frac{1}{9}} t^{\frac{1}{6}}, \tag{5.8}$$

respectively. Since all of the parameter-dependent factors are $\mathcal{O}(1)$ for the potentials presented in this paper and ref. [1], it is straightforward to see that the first constraint is easily satisfied but the second only marginally so. Without a systematic way of computing corrections to high orders, one cannot be sure of the degree of accuracy of the non-perturbative potential presented here. However, attempts to compute the next to leading order corrections — for a concrete example see appendix D of ref. [51] — suggest that there is not a qualitative change in the physics implications.

5.4 Additional consistency conditions on theories with extra dimensions

Even if the Swampland conjectures are satisfied for the potentials derived here, there are generic "metric-based" consistency conditions that must also be satisfied by theories with extra spatial dimensions [24–26], including our heterotic M-theory models.

The Swampland and metric based constraints are fundamentally different in character. Whereas the Swampland conjectures impose constraints on potential shapes independent of cosmology, the metric-based consistency conditions are based on the equation of state of the universe independent of the potential shape. The metric-based conditions apply

JHEP07(2024)288

to any compactified theory with a Ricci-flat or conformally Ricci-flat metric that satisfies the null energy condition (NEC). This includes Type 2 potentials (or Type 5 models if $V > 0$ at the minimum), as well as non-string theoretic examples, such as Randall-Sundrum. The conditions only become relevant in our examples if the universe undergoes a period of accelerated expansion due to being trapped in the metastable vacuum with $V > 0$. Then, as shown in ref. [24], it is impossible to satisfy the Einstein equations in both higher dimensions and in the effective (3+1)-dimensional compactified theory. In the case of Type 2 potentials (or Type 5 models if $V > 0$ at the minimum), if the universe becomes trapped in the metastable phase and the extra dimensions do not decompactify, the null energy condition must be violated with a time-varying component that is inhomogeneously distributed in the compact dimensions and that is varying in synchrony with w, the equation-of-state in the (3+1)-d effective theory [26].

The heterotic M-theory models considered here do not include an exotic NEC-violating ingredient of this kind. If there is no such component, a prediction is that decompactification must begin and/or deviations from the Einstein equations must start to grow large. The current phase of dark energy domination and accelerated expansion cannot be maintained for more than a few e-folds into the future without these producing an observable effect.

6 Final remarks

We close by pointing out the remarkable example of the Type 5 heterotic M-theory potential with $V \approx 0$ at the minimum. This example satisfied all the constraints we have considered. First, it was derived from 11d M-theory following a protocol full of intricate steps. Second, we have shown the highly non-trivial result that it can be combined with a visible sector that leads to realistic particle phenomenology. Third, the model is consistent with ΛCDM cosmology or, with a modest enhancement, quintessence dark energy replacing the cosmological constant Λ. In the latter case, where $V = 0$ precisely at the minimum, there need not be a long-lasting period of accelerated expansion, so the metric-based constraints can be satisfied. Unlike all the other examples, the vacuum state is globally stable and eternal. (The cases with negative potential minima are unstable to gravitational collapse and have a finite lifetime; the cases with positive minima are metastable and have a finite lifetime.) The vacuum in Type 5 models is supersymmetry breaking but never decays to the supersymmetric vacuum at $\langle t \rangle \to \infty$ where extra dimensions open up. We believe that the existence of a heterotic M-theory model possessing all these properties is quite noteworthy.

Acknowledgments

We thank Alek Bedroya and Cumrun Vafa for many useful comments. Burt Ovrut is supported in part by both the research grant DOE No. DESC0007901 and SAS Account 020-0188-2-010202-6603-0338. Ovrut would like to ac- knowledge the hospitality of the CCPP at New York University where much of this work was carried out. Paul Steinhardt is supported in part by the DOE grant number DEFG02-91ER40671 and by the Simons Foundation grant number 654561. Steinhardt thanks the Cumrun Vafa and the High Energy Physics group in the Department of Physics at Harvard University for graciously hosting him during his sabbatical leave.

JHEP07(2024)288

References

[1] C. Deffayet, B.A. Ovrut and P.J. Steinhardt, *Moduli axions, stabilizing moduli, and the large field swampland conjecture in heterotic M-theory*, *Phys. Rev. D* **109** (2024) 126004 [arXiv:2312.04656] [INSPIRE].

[2] A. Bedroya and C. Vafa, *Trans-Planckian Censorship and the Swampland*, *JHEP* **09** (2020) 123 [arXiv:1909.11063] [INSPIRE].

[3] H. Ooguri and C. Vafa, *On the Geometry of the String Landscape and the Swampland*, *Nucl. Phys. B* **766** (2007) 21 [hep-th/0605264] [INSPIRE].

[4] H. Ooguri, E. Palti, G. Shiu and C. Vafa, *Distance and de Sitter Conjectures on the Swampland*, *Phys. Lett. B* **788** (2019) 180 [arXiv:1810.05506] [INSPIRE].

[5] D. Lüst, E. Palti and C. Vafa, *AdS and the Swampland*, *Phys. Lett. B* **797** (2019) 134867 [arXiv:1906.05225] [INSPIRE].

[6] E. Palti, *The Swampland: Introduction and Review*, *Fortsch. Phys.* **67** (2019) 1900037 [arXiv:1903.06239] [INSPIRE].

[7] P. Horava and E. Witten, *Eleven-dimensional supergravity on a manifold with boundary*, *Nucl. Phys. B* **475** (1996) 94 [hep-th/9603142] [INSPIRE].

[8] P. Horava and E. Witten, *Heterotic and Type I string dynamics from eleven dimensions*, *Nucl. Phys. B* **460** (1996) 506 [hep-th/9510209] [INSPIRE].

[9] A. Lukas, B.A. Ovrut, K.S. Stelle and D. Waldram, *The Universe as a domain wall*, *Phys. Rev. D* **59** (1999) 086001 [hep-th/9803235] [INSPIRE].

[10] A. Lukas, B.A. Ovrut, K.S. Stelle and D. Waldram, *Heterotic M theory in five-dimensions*, *Nucl. Phys. B* **552** (1999) 246 [hep-th/9806051] [INSPIRE].

[11] T. Banks and M. Dine, *Couplings and scales in strongly coupled heterotic string theory*, *Nucl. Phys. B* **479** (1996) 173 [hep-th/9605136] [INSPIRE].

[12] A. Lukas, B.A. Ovrut and D. Waldram, *On the four-dimensional effective action of strongly coupled heterotic string theory*, *Nucl. Phys. B* **532** (1998) 43 [hep-th/9710208] [INSPIRE].

[13] V. Braun, Y.-H. He, B.A. Ovrut and T. Pantev, *The exact MSSM spectrum from string theory*, *JHEP* **05** (2006) 043 [hep-th/0512177] [INSPIRE].

[14] L.B. Anderson, J. Gray, A. Lukas and E. Palti, *Heterotic standard models from smooth Calabi-Yau three-folds*, *PoS* **CORFU2011** (2011) 096 [INSPIRE].

[15] L.B. Anderson, J. Gray, A. Lukas and E. Palti, *Two Hundred Heterotic Standard Models on Smooth Calabi-Yau Threefolds*, *Phys. Rev. D* **84** (2011) 106005 [arXiv:1106.4804] [INSPIRE].

[16] L.B. Anderson, J. Gray, A. Lukas and E. Palti, *Heterotic Line Bundle Standard Models*, *JHEP* **06** (2012) 113 [arXiv:1202.1757] [INSPIRE].

[17] M. Cicoli et al., *The Standard Model quiver in de Sitter string compactifications*, *JHEP* **08** (2021) 109 [arXiv:2106.11964] [INSPIRE].

[18] S. Gukov, S. Kachru, X. Liu and L. McAllister, *Heterotic moduli stabilization with fractional Chern-Simons invariants*, *Phys. Rev. D* **69** (2004) 086008 [hep-th/0310159] [INSPIRE].

JHEP07(2024)288

[19] V. Balasubramanian, P. Berglund, J.P. Conlon and F. Quevedo, *Systematics of moduli stabilisation in Calabi-Yau flux compactifications*, *JHEP* **03** (2005) 007 [hep-th/0502058] [INSPIRE].

[20] L.B. Anderson, J. Gray, A. Lukas and B. Ovrut, *Stabilizing All Geometric Moduli in Heterotic Calabi-Yau Vacua*, *Phys. Rev. D* **83** (2011) 106011 [arXiv:1102.0011] [INSPIRE].

[21] M. Cicoli, S. de Alwis and A. Westphal, *Heterotic Moduli Stabilisation*, *JHEP* **10** (2013) 199 [arXiv:1304.1809] [INSPIRE].

[22] E.I. Buchbinder and B.A. Ovrut, *Vacuum stability in heterotic M theory*, *Phys. Rev. D* **69** (2004) 086010 [hep-th/0310112] [INSPIRE].

[23] B. Fraiman, M. Graña, H. Parra De Freitas and S. Sethi, *Non-Supersymmetric Heterotic Strings on a Circle*, arXiv:2307.13745 [INSPIRE].

[24] P.J. Steinhardt and D. Wesley, *Dark Energy, Inflation and Extra Dimensions*, *Phys. Rev. D* **79** (2009) 104026 [arXiv:0811.1614] [INSPIRE].

[25] P.J. Steinhardt and D. Wesley, *Exploring extra dimensions through observational tests of dark energy and varying Newton's constant*, arXiv:1003.2815 [INSPIRE].

[26] G. Montefalcone, P.J. Steinhardt and D.H. Wesley, *Dark energy, extra dimensions, and the Swampland*, *JHEP* **06** (2020) 091 [arXiv:2005.01143] [INSPIRE].

[27] P. Candelas and X. de la Ossa, *Moduli Space of Calabi-Yau Manifolds*, *Nucl. Phys. B* **355** (1991) 455 [INSPIRE].

[28] J. Gray, A. Lukas and B. Ovrut, *Flux, gaugino condensation and anti-branes in heterotic M-theory*, *Phys. Rev. D* **76** (2007) 126012 [arXiv:0709.2914] [INSPIRE].

[29] M. Dine, R. Rohm, N. Seiberg and E. Witten, *Gluino Condensation in Superstring Models*, *Phys. Lett. B* **156** (1985) 55 [INSPIRE].

[30] H.P. Nilles, *Gaugino Condensation and Supersymmetry Breakdown*, *Int. J. Mod. Phys. A* **5** (1990) 4199 [INSPIRE].

[31] P. Horava, *Gluino condensation in strongly coupled heterotic string theory*, *Phys. Rev. D* **54** (1996) 7561 [hep-th/9608019] [INSPIRE].

[32] A. Lukas, B.A. Ovrut and D. Waldram, *Gaugino condensation in M theory on S^1/Z_2*, *Phys. Rev. D* **57** (1998) 7529 [hep-th/9711197] [INSPIRE].

[33] M. Dine, N. Seiberg, X.G. Wen and E. Witten, *Nonperturbative Effects on the String World Sheet*, *Nucl. Phys. B* **278** (1986) 769 [INSPIRE].

[34] M. Dine, N. Seiberg, X.G. Wen and E. Witten, *Nonperturbative Effects on the String World Sheet. II*, *Nucl. Phys. B* **289** (1987) 319 [INSPIRE].

[35] E. Witten, *Nonperturbative superpotentials in string theory*, *Nucl. Phys. B* **474** (1996) 343 [hep-th/9604030] [INSPIRE].

[36] G. Curio, *On the Heterotic World-sheet Instanton Superpotential and its individual Contributions*, *JHEP* **08** (2010) 092 [arXiv:1006.5568] [INSPIRE].

[37] V. Braun, M. Kreuzer, B.A. Ovrut and E. Scheidegger, *Worldsheet instantons and torsion curves, part A: Direct computation*, *JHEP* **10** (2007) 022 [hep-th/0703182] [INSPIRE].

[38] V. Braun, M. Kreuzer, B.A. Ovrut and E. Scheidegger, *Worldsheet instantons, torsion curves, and non-perturbative superpotentials*, *Phys. Lett. B* **649** (2007) 334 [hep-th/0703134] [INSPIRE].

JHEP07(2024)288

[39] E.I. Buchbinder, R. Donagi and B.A. Ovrut, *Superpotentials for vector bundle moduli*, *Nucl. Phys. B* **653** (2003) 400 [hep-th/0205190] [INSPIRE].

[40] G. Curio, *Perspectives on Pfaffians of Heterotic World-sheet Instantons*, *JHEP* **09** (2009) 131 [arXiv:0904.2738] [INSPIRE].

[41] C. Beasley and E. Witten, *Residues and world sheet instantons*, *JHEP* **10** (2003) 065 [hep-th/0304115] [INSPIRE].

[42] E. Buchbinder, A. Lukas, B. Ovrut and F. Ruehle, *Heterotic Instanton Superpotentials from Complete Intersection Calabi-Yau Manifolds*, *JHEP* **10** (2017) 032 [arXiv:1707.07214] [INSPIRE].

[43] E.I. Buchbinder, L. Lin and B.A. Ovrut, *Non-vanishing Heterotic Superpotentials on Elliptic Fibrations*, *JHEP* **09** (2018) 111 [arXiv:1806.04669] [INSPIRE].

[44] E.I. Buchbinder, A. Lukas, B.A. Ovrut and F. Ruehle, *Heterotic Instantons for Monad and Extension Bundles*, *JHEP* **02** (2020) 081 [arXiv:1912.07222] [INSPIRE].

[45] E.I. Buchbinder, A. Lukas, B.A. Ovrut and F. Ruehle, *Instantons and Hilbert Functions*, *Phys. Rev. D* **102** (2020) 026019 [arXiv:1912.08358] [INSPIRE].

[46] E.I. Buchbinder and B.A. Ovrut, *Non-vanishing Superpotentials in Heterotic String Theory and Discrete Torsion*, *JHEP* **01** (2017) 038 [arXiv:1611.01922] [INSPIRE].

[47] S. Dumitru and B.A. Ovrut, *Heterotic M-Theory Hidden Sectors with an Anomalous $U(1)$ Gauge Symmetry*, arXiv:2109.13781 [INSPIRE].

[48] S. Dumitru and B.A. Ovrut, *Moduli and Hidden Matter in Heterotic M-Theory with an Anomalous $U(1)$ Hidden Sector*, arXiv:2201.01624 [INSPIRE].

[49] M.B. Green and J.H. Schwarz, *Anomaly Cancellation in Supersymmetric $D = 10$ Gauge Theory and Superstring Theory*, *Phys. Lett. B* **149** (1984) 117 [INSPIRE].

[50] D.Z. Freedman and A. Van Proeyen, *Supergravity*, Cambridge University Press (2012) [DOI:10.1017/cbo9781139026833].

[51] A. Ashmore, S. Dumitru and B.A. Ovrut, *Line Bundle Hidden Sectors for Strongly Coupled Heterotic Standard Models*, *Fortsch. Phys.* **69** (2021) 2100052 [arXiv:2003.05455] [INSPIRE].

[52] R. Deen, B.A. Ovrut and A. Purves, *The minimal SUSY $B - L$ model: simultaneous Wilson lines and string thresholds*, *JHEP* **07** (2016) 043 [arXiv:1604.08588] [INSPIRE].

[53] A. Ashmore, S. Dumitru and B.A. Ovrut, *Explicit soft supersymmetry breaking in the heterotic M-theory $B - L$ MSSM*, *JHEP* **08** (2021) 033 [arXiv:2012.11029] [INSPIRE].

[54] V. Braun, Y.-H. He, B.A. Ovrut and T. Pantev, *A heterotic standard model*, *Phys. Lett. B* **618** (2005) 252 [hep-th/0501070] [INSPIRE].

[55] B.A. Ovrut, A. Purves and S. Spinner, *The minimal SUSY $B - L$ model: from the unification scale to the LHC*, *JHEP* **06** (2015) 182 [arXiv:1503.01473] [INSPIRE].

[56] A. Bedroya, *Holographic origin of TCC and the distance conjecture*, *JHEP* **06** (2024) 016 [arXiv:2211.09128] [INSPIRE].

[57] D. van de Heisteeg, C. Vafa, M. Wiesner and D.H. Wu, *Bounds on field range for slowly varying positive potentials*, *JHEP* **02** (2024) 175 [arXiv:2305.07701] [INSPIRE].

JHEP07(2024)288